NANO LETTERS

LETTER

pubs.acs.org/NanoLett

Oxidative Doping Renders Graphene Hydrophilic, Facilitating Its Use As a Support in Biological TEM

Radosav S. Pantelic,*,† Ji Won Suk,‡ Yufeng Hao,‡ Rodney S. Ruoff,*,‡ and Henning Stahlberg*,†

†Center for Cellular Imaging and NanoAnalytics, Biozentrum, University of Basel, Basel, Switzerland

‡Department of Mechanical Engineering and Materials Science and Engineering Program, The University of Texas, Austin, Texas, United States

ABSTRACT: Graphene represents the first practical realization of crystalline supports in biological transmission electron microscopy (TEM) since their introduction over 30 years ago. The high transparency, minimal inelastic cross-section, and electrical conductivity of graphene are highly desirable characteristics for a TEM support. However, without a suitable method for rendering graphene supports, hydrophilic applications are limited. This work describes the in situ functionalization of graphene with minimal structural degradation, rendering TEM supports sufficiently hydrophilic for the mounting of biological samples.

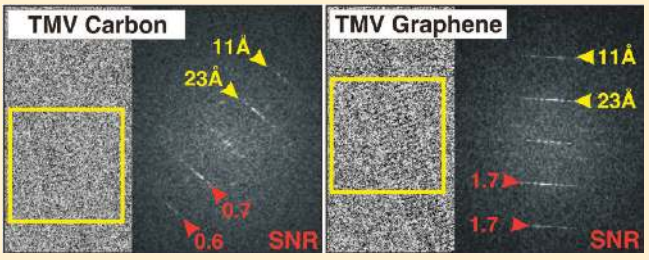

KEYWORDS: Graphene, electron microscopy, cryo-EM, crystallography

Evaporated carbon supports have long been used in the imaging of biological molecules by transmission electron microscopy (TEM). However, amorphous carbon imposes a strong background signal that attenuates or may completely obstruct that of unstained molecules. Although the imaging of molecules within freestanding areas of vitreous ice is generally the most preferable method,[1] specific techniques and difficult samples often require the addition of a thin amorphous carbon support. Crystalline supports offer an interesting alternative,[2,3] as they are essentially transparent down to the resolution of their periodicity regardless of thickness. And even at resolutions higher than the lattice constant of the supporting film, the crystalline signal from the film can be computationally removed from images.[4] However, complicated and limited-scale preparation has so far prevented the use of thin crystalline supports in biological TEM.

Graphene has renewed interest in crystalline TEM supports,[5−11] and the large-scale synthesis of continuous graphene by chemical vapor deposition (CVD)[12] has made graphene TEM supports feasible. Graphene offers three key advantages: Pristine graphene is essentially featureless and electron transparent down to a resolution of 2.13 Å (well outside resolutions currently resolved by most biological TEM investigations). Furthermore, at 0.34 nm single-layer (single atom) thickness,[13] background amplitude (noise) attributed to inelastic and multiple electron scattering within the support is minimized. Graphene also demonstrates electrical conductivity several orders of magnitude greater than that of amorphous carbon[14−16] and may therefore reduce sample charging and drift.

Our earlier work demonstrated the preparation of vitrified protein samples across graphene oxide supports.[17] Despite coarse attenuation by chemically introduced functional groups, the enhanced transmission properties of graphene oxide approach those of pristine graphene and supports readily attach biological molecules. However, random variations in thickness and coverage by deposition of individual graphene oxide platelets from solution were a fundamental drawback of the method, which limited the feasibility of graphene oxide TEM supports. Furthermore, graphene oxide behaves largely as an electrical insulator.[18] Continuous, single-layer pristine graphene produced by chemical vapor deposition (CVD) addresses these limitations. In subsequent work we described the transfer of continuous, single-layer graphene supports and compared the transmission properties of pristine graphene to graphene oxide and thin amorphous carbon in detail.[19] Free from coarse oxidization, pristine graphene demonstrated significantly higher transparency and is electrically conductive. However, the hydrophobic properties of pristine graphene prevent the direct adsorption of biological molecules. Hence, the application of pristine graphene supports in biological TEM has to date been limited.

Amorphous carbon supports are traditionally rendered hydrophilic by exposure to ion plasma, by which incident ions disrupt the surface allowing introduction of −OH and C═O groups (for example). This method is not suitable for graphene, as incident ions extensively damage individual graphene layers. In this manuscript we present a method by which graphene supports are rendered sufficiently hydrophilic for biological TEM, with minimal structural damage or attenuation of properties.

Received: July 13, 2011
Revised: August 29, 2011

dx.doi.org/10.1021/nl202386p | *Nano Lett.* XXXX, XXX, 000–000

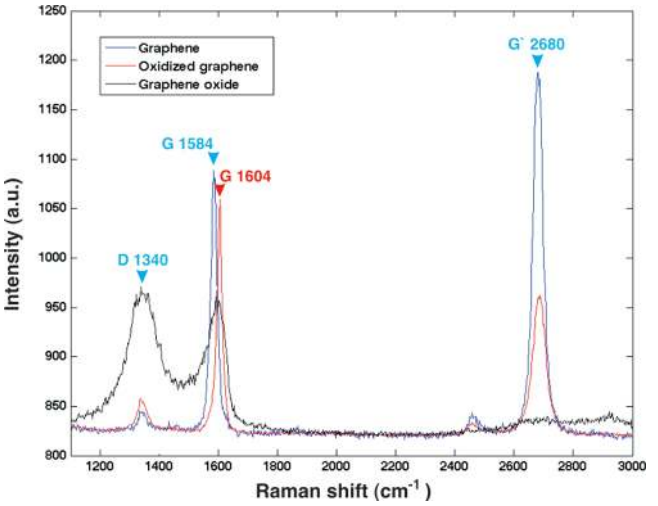

Figure 1. Comparison of the minimal structural changes induced by functionalization: Raman spectra of CVD graphene before (blue) and after functionalization (red) as well as graphene oxide (black) are compared. Typical graphene structure is indicated by the positions of the D, G, and G′ peaks at ∼1340, ∼1584, and ∼2680 cm^{-1}, respectively (blue markers). Shifting of the G mode (red markers) by up to 20 cm^{-1} and significant increase of $I_G/I_{G'}$ ratio indicate partial oxidation by doping. The graphene structure is otherwise minimally changed, as emphasized upon comparison to graphene oxide (note D intensities).

An unrelated study reported the etching of single and multilayer graphene during high-temperature oxidative annealing.[20] At fixed oxygen and argon gas flows, graphene samples were heated to different temperatures over fixed 2 h periods.[20] At temperatures as low as 200−300 °C, Raman spectroscopy indicated oxidative doping of the graphene, and atomic force microscopy failed to discern any etching of single-layer graphene at 400 °C and below.[20] Hence, we here applied oxidative annealing to graphene in order to prepare hydrophilic TEM support films.

Raman spectroscopy facilitates the comparison of graphene structure according to the position and the intensity of characteristic peaks. Figure 1 shows Raman spectra from single layer CVD graphene before (blue) and after functionalization (red, 2 h at 375 °C). Graphene is characterized by an absent or minimal D peak at ∼1340 cm^{-1} (indicating a negligible or small proportion of structural defects), a G peak at ∼1584 cm^{-1} and a G′ peak at ∼2680 cm^{-1} (Figure 1, blue markers). After functionalization by oxygen doping, the sample shows an up-shifted G mode (red marker), as also previously reported.[20] Specifically, the ∼20 cm^{-1} G peak shift and significant increase of $I_G/I_{G'}$ ratio indicate partial oxidation by doping.

The negligible D peak intensity after functionalization (Figure 1, red, I_D/I_G= ∼0.14) indicates minimal structural damage and is comparable to occasional growth defects found in single-layer CVD samples (Figure 1, blue).[21] In contrast, graphene oxide (Figure 1, black) demonstrates particularly high defect ratios (I_D/I_G= ∼1.01) and an almost absent G′ peak after extensive structural damage by harsh chemical oxidization. Also experimenting with additional preannealing at 400 °C in reducing atmosphere (Ar/H_2 mixture), we often observed a significant widening of the D peak (data not shown) implying the amorphous carbonization of residual polymers remaining (despite washing in solvent) after polymer-assisted transfer of the graphene. This background is not present after functionalization,

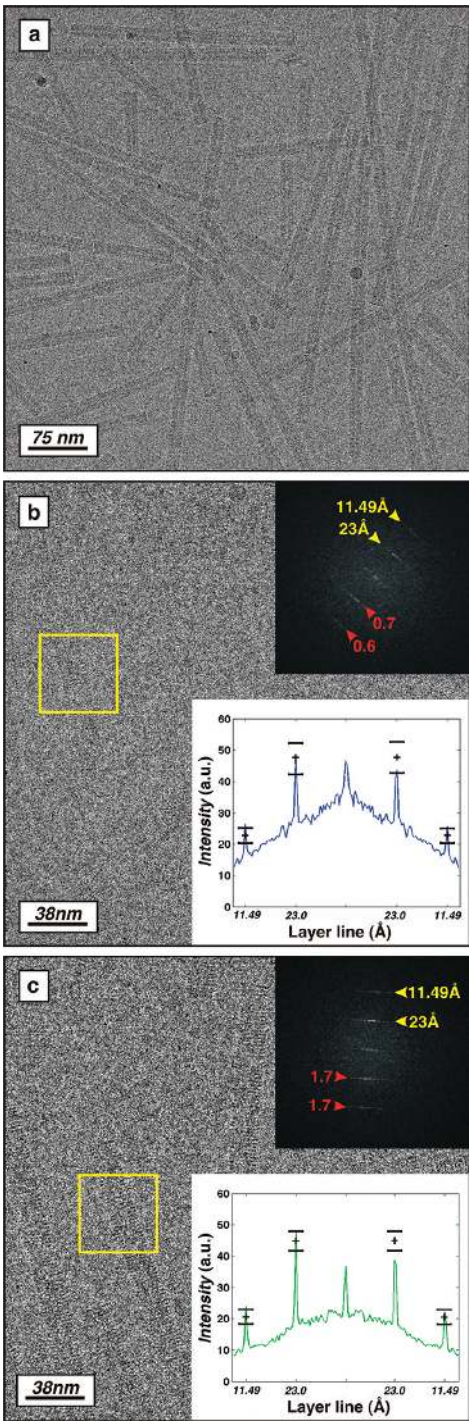

Figure 2. Comparison of SNR by examination of TMV layer lines: TMV was imaged across freestanding areas of 2 nm thick amorphous carbon (b) and single-layer graphene (a, c). Panel (a) shows a representative area of the functionalized graphene (2 μm defocus), abound with TMV despite several washes and relatively low sample concentration (∼0.1 mg/mL). The transparency of either support can be compared by the SNR's of the third- and sixth-order layer lines in the Fourier transform (panels a and b insets; lattice lines at ∼23.0 and ∼11.49 Å are indicated by yellow markers and the corresponding SNR in red) and corresponding profile plots (error bars indicate 1 standard deviation outside the mean intensity of each layer line calculated across the data set). Yellow boxes in panels (b) and (c) denote a section of TMV.

dx.doi.org/10.1021/nl202386p |*Nano Lett.* XXXX, XXX, 000–000

most likely as the amorphous carbon deposits are converted to CO and/or CO_2 during oxidative annealing. Interestingly, the functionalized graphene also remains conductive. Although average sheet resistance across several oxygen-doped samples (van der Pauw method) increased over 5-fold (from ~0.86 to ~4.7 kΩ/cm^2) after functionalization, it is worth noting that graphene oxide behaves largely as an insulator.[18]

Low-dose images of unstained tobacco mosaic virus (TMV) vitrified across functionalized graphene demonstrate the suitability of the new method in preparing protein samples (Figure 2).[22] Note that despite several washes and relatively low sample concentration (~0.1 mg/mL), TMV is present in abundance across the functionalized graphene support (Figure 2a). The periodic structure of TMV manifests itself as diffracted layer lines in the Fourier transform (of which the third and sixth order are most relevant as they relate to higher resolution structure), the signal-to-noise ratios (SNR) of which have been used in a further practical demonstration of the graphene support's high transparency.

For comparison, ~260 micrographs of frozen hydrated TMV on 2 nm thick amorphous carbon films were recorded. One such image demonstrating the highest SNR at the sixth-order layer line is reproduced in Figure 2b. The average Fourier transform (Figure 2b, top inset) features the third- and sixth-order layer lines (at ~23.0 and ~11.49 Å^{-1}, respectively) with respective SNR's of 0.7 and 0.6. The accompanying profile plot (Figure 2b, bottom inset) shows the relative intensity of each layer line (error bars indicate 1 standard deviation outside the mean intensity calculated across all Fourier transforms, demonstrating information up to the sixth-order layer line). The average SNR of the third- and sixth-order layer lines across the TMV/carbon data were 0.9 and 0.53, respectively.

We then recorded a set of ~270 micrographs of frozen hydrated TMV mounted on treated graphene. One such image is shown in Figure 2c. The calculated Fourier transform (Figure 2c, top inset) demonstrates third- and sixth-order layer lines with significantly higher SNR's (both at 1.7). The significant reduction in background is clearly seen in the accompanying profile plot. On average, the calculated SNR's of either layer line were much higher at 1.48 and 1.02 (third and sixth, respectively).

The large-scale preparation of graphene by CVD has facilitated a practical realization of crystalline TEM supports, first proposed over 30 years ago with cleaved graphite and vermiculite supports.[2,3] To our knowledge this is the first demonstration of a suitable method for rendering graphene supports hydrophilic (with minimal attenuation of the inherent imaging properties), enabling the mounting of biological molecules. The transparency, minimal scattering cross-section, and electrical conductivity of monolayer graphene make it the ideal support for TEM. It is anticipated that this method will facilitate the wide use of graphene supports in biological TEM and accommodate high-resolution studies. The improved signal-to-noise ratios offered by graphene will improve the imaging of low-mass, unstained proteins, and other methods requiring additional carbon support (e.g., electron crystallography, time-resolved cryo-EM, difficult low-concentration samples, and other emerging techniques).[23,24,10,25,6] The increased conductivity of graphene supports may also improve imaging stability. This method is also relevant outside TEM and may contribute to other applications seeking to attach biological material to graphene, such as the development of organic sensors and devices.

EXPERIMENTAL SECTION

Physical Characterization of the Graphene. Copper foils covered on both sides with CVD graphene[21,26,27] were pre-etched for 90s with 5% w/v nitric acid to remove one of the graphene layers before spin coating the remaining layer (40s at 4000 rpm) with poly(methyl methacrylate) (PMMA, 20 mg/mL concentration in 99.9% chlorobenzene). The PMMA/graphene backed Cu foils were floated across 0.3 M of ammonium persulfate solution and etched overnight. After several washes with distilled water, the ~1 cm^2 PMMA backed graphene samples were transferred onto SiO_2 (285 nm thick) /Si substrates and dried in a vacuum desiccator overnight.[28]

Raman spectra (WITec alpha300, 532 nm laser, 100× objective) were collected before and after annealing/oxidization, as were sheet resistances (4-probe van der Pauw method). The graphene/SiO_2 samples were oxidized in a 25 mm quartz glass tube furnace for 2 h at given temperatures between 200 and 375 °C (to assess any damage from possible etching) under combined O_2/Ar gas flows of ~0.20 and ~0.18 L/min, respectively. Some samples were also preannealed at 400 °C for 1 h under constant H_2/Ar flow (reducing atmosphere, ~0.20 and ~0.18 L/min, respectively), although this was later deemed unnecessary after comparing Raman spectra. We further experimented with higher O_2 gas ratios but failed to observe any changes to the degree of functionalization.

TEM Sample Preparation. Monolayer graphene alone will not span bare TEM grids and requires an additional scaffold. CVD graphene[21,26,27] was transferred to 1.2/1.3 μm Quantifoil TEM grids (Quantifoil Micro Tools GmbH, Jena, Germany), according to our previous method,[19] and spans the periodic holes of the amorphous carbon film (the thick amorphous carbon is also used for focusing). Since our previous work, we have found that etching with 0.3 M of ammonium persulfate solution produces significantly cleaner graphene samples.[29]

Using a purpose built furnace, transferred graphene TEM supports were heated to 300 °C in ~0.15 L/min of O_2/Ar (33/66% mixture) gas flow for 2 h before cooling to room temperature (also under gas flow). During this time, the temperature was slowly ramped (and limited to 300 °C) to prevent/minimize any tearing of the carbon Quantifoil support by the slightly different expansion coefficients of the Au TEM grid and amorphous carbon scaffold.

Vitrified samples were prepared with TMV diluted in buffer (1 mM of EDTA, pH of 7.7) to a final concentration of ~0.1 mg/mL. With no further preparation of the functionalized graphene, 5 μL of sample was applied and left to incubate for ~2 min before washing the grid 2−3 times by buffer exchange with phosphate-buffered saline. Washing was used as a control to ensure that the sample had in fact attached to the graphene in sufficient concentration. Using an FEI Vitrobot Mark IV, grids were blotted for 2 s at 10 °C and 100% humidity before plunging into liquid ethane. TMV was also prepared across 2 nm thick amorphous carbon film according to the same parameters. Such 2 nm amorphous carbon supports are commercially available spanning 1.2/1.3 μm Quantifoil for additional physical stability (Quantifoil Micro Tools GmbH, Jena, Germany).

Imaging. Unstained, vitrified TMV (Figure 2) was imaged at low dose (<30 e/Å^2) across freestanding areas of 2 nm of amorphous carbon and functionalized graphene using an FEI Titan KRIOS operated at 300 keV. Data were recorded to a CCD camera (Gatan Ultrascan 4000, 15 μm physical pixel size) at 59 000× magnification (1.47 Å pixel size) and 0.5s exposure time.

dx.doi.org/10.1021/nl202386p |Nano Lett. XXXX, XXX, 000–000

In a practical demonstration of the support's transparency, we compared the signal-to-noise ratios (SNR) of layer lines diffracted by the periodic structure of TMV. A total of ~530 micrographs (~260 amorphous carbon and ~270 graphene) were acquired using EPU automated single particle acquisition software (FEI Company, Netherlands) over a range of fixed defoci (1.1–1.4 μm). The theoretical zero-crossings of the CTF at each defocus were calculated and checked so as not to coincide with the third- and sixth-order layer lines of TMV at ~23.0 and ~11.49 Å, respectively. All micrographs were normalized, and average Fourier transforms (Figure 2, insets) were calculated from 5 partially overlapping, 512 × 512 pixel boxes sampled along individual TMV fibres.

Taking ice thickness into consideration, we sought to image areas with the thinnest possible ice (particularly in the case of the thicker amorphous carbon support). Grid squares with similar ice thickness between each sample were selected (according to the blotting gradients apparent across each grid at low magnification) from which the automated acquisition software acquired targets according to ice thickness.

AUTHOR INFORMATION

Corresponding Author

*E-mail: Radosav.Pantelic@unibas.ch; R.Ruoff@mail.utexas.edu; Henning.Stahlberg@unibas.ch.

ACKNOWLEDGMENT

TMV was a kind gift from Dr. Ruben Diaz-Avalos (New York Structural Biology Center, USA) and Dr Philippe Ringler (C-CINA, Basel, Switzerland). We thank Gerardo Algara-Siller and Prof. Ute Kaiser (Group of Electron Microscopy of Materials Science, Central Facility of Electron Microscopy, University of Ulm, Ulm, Germany) for their assistance in the investigation of doped samples by Cs corrected TEM. The group of Prof. Rod Ruoff appreciates support from NSF award no. 0969106 and the Office of Naval Research. This work was in part supported by the Swiss initiative for Systems Biology (SystemsX.ch, grant CINA) and the Swiss National Science Foundation (NCCR TransCure, NCCR Structural Biology, and NCCR Nano).

REFERENCES

(1) Dubochet, J; Adrian, M; Chang, J-J; Homo, J-C; Lepault, J; McDowall, A. W.; Schultz, P Cryo-electron microscopy of vitrified specimens. *Q. Rev. Biophys.* **1988**, *21*, 129–228.

(2) Hahn, M; Baumeister, W High resolution negative staining of ferritin molecules on vermiculite single crystal supports. *Biochim. Biophys. Acta* **1974**, *371* (1), 267.

(3) Dobelle, W. H.; Beer, M Chemically cleaved graphite support films for electron microscopy. *J. Cell Biol.* **1968**, *39* (3), 733–735.

(4) Wang, L; Sigworth, F. J. Structure of the BK potassium channel in a lipid membrane from electron cryomicroscopy. *Nature* **2009**, *461* (7261), 292–295.

(5) Mitsuoka, K Obtaining high-resolution images of biological macromolecules by using a cryo-electron microscope with a liquid-helium cooled stage. *Micron* **2011**, *42* (2), 100–106.

(6) Benesch, J. L. P.; Ruotolo, B. T.; Simmons, D. A.; Barrera, N. P.; Morgner, N; Wang, L; Saibil, H. R.; Robinson, C. V. Separating and visualising protein assemblies by means of preparative mass spectrometry and microscopy. *J. Struct. Biol.* **2010**, *172* (2), 161–168.

(7) Massover, W. H. New and unconventional approaches for advancing resolution in biological transmission electron microscopy by improving macromolecular specimen preparation and preservation. *Micron* **2011**, *42* (2), 141–151.

(8) Mutus, J. Y.; Livadaru, L; Robinson, J. T.; Urban, R; Salomons, M. H.; Cloutier, M; Wolkow, R. A. Low-energy electron point projection microscopy of suspended graphene, the ultimate 'microscope slide'. *New J. Phys.* **2011**, *13* (6), 063011.

(9) Westenfelder, B; Meyer, J. C.; Biskupek, J; Algara-Siller, G; Lechner, L. G.; Kusterer, J; Kaiser, U; Krill, C. E.; Kohn, E; Scholz, F Graphene-based sample supports for in situ high-resolution TEM electrical investigations. *J. Phys. D: App. Phys.* **2011**, *44* (5), 055502.

(10) Liu, Z; Jiang, L; Galli, F; Nederlof, I; Olsthoorn, R. C. L.; Lamers, G. E. M.; Oosterkamp, T. H.; Abrahams, J. P. A. Graphene OxidėStreptavidin Complex for Biorecognition — Towards Affinity Purification. *Adv. Funct. Mater.* **2010**, *20* (17), 2857–2865.

(11) Rhinow, D; Enfeld, M. B.; Weber, N. E.; Beyer, A; Goelzhaeuser, A; Kuehlbrandt, W; Hampp, N; Turchanin, A Energy-filtered transmission electron microscopy of biological samples on highly transparent carbon nanomembranes. *Ultramicroscopy* **2011**, *111* (5), 342–349.

(12) Li, X. S.; Cai, W. W.; An, J. H.; Kim, S; Nah, J; Yang, D. X.; Piner, R; Velamakanni, A; Jung, I; Tutuc, E; Banerjee, S. K.; Colombo, L; Ruoff, R. S. Large-Area Synthesis of High-Quality and Uniform Graphene Films on Copper Foils. *Science* **2009**, *324* (5932), 1312–1314.

(13) Eda, G; Fanchini, G; Chhowalla, M Large-area ultrathin films of reduced graphene oxide as a transparent and flexible electronic material. *Nat. Nanotechnol.* **2008**, *3* (5), 270–274.

(14) Chen, J. H.; Jang, C; Adam, S; Fuhrer, M. S.; Williams, E. D.; Ishigami, M Charged-impurity scattering in graphene. *Nat. Phys.* **2008**, *4* (5), 377–381.

(15) Robertson, J Amorphous carbon. *Adv. Phys.* **1986**, *35* (4), 317–374.

(16) Ziegler, K Robust transport properties in graphene. *Phys. Rev. Lett.* **2006**, *97* (26), 266802.

(17) Pantelic, R; Meyer, J; Kaiser, U; Baumeister, W; Plitzko, J Graphene oxide: A substrate for optimizing preparations of frozen-hydrated samples. *J. Struct. Biol.* **2009**, *170*, 152–156.

(18) Jung, I; Dikin, D. A.; Piner, R. D.; Ruoff, R. S. Tunable Electrical Conductivity of Individual Graphene Oxide Sheets Reduced at Low Temperatures. *Nano Lett.* **2008**, *8* (12), 4283–4287.

(19) Pantelic, R; Suk, J. W.; Magnuson, C. W.; Meyer, J. C.; Wachsmuth, P; Kaiser, U; Ruoff, R. S.; Stahlberg, H Graphene: Substrate preparation and introduction. *J. Struct. Biol.* **2011**, *174* (1), 234–238.

(20) Liu, L; Ryu, S; Tomasik, M; Stolyarova, E; Jung, N; Hybertsen, M; Steigerwald, M; Brus, L; Flynn, G Graphene oxidation: Thickness-dependent etching and strong chemical doping. *Nano Lett.* **2008**, *8* (7), 1965–1970.

(21) Li, X; Cai, W; Colombo, L; Ruoff, R. S. Evolution of Graphene Growth on Ni and Cu by Carbon Isotope Labeling. *Nano Lett.* **2009**, *9* (12), 4268–4272.

(22) Sachse, C; Chen, J. Z.; Coureux, P. D.; Stroupe, M. E.; Fandrich, M; Grigorieff, N High-resolution electron microscopy of helical specimens: a fresh look at tobacco mosaic virus. *J. Mol. Biol.* **2007**, *371* (3), 812–835.

(23) Stahlberg, H; Walz, T Molecular electron microscopy: state of the art and current challenges. *ACS Chem. Biol.* **2008**, *3* (5), 268–281.

(24) Evans, J. E.; Jungjohann, K. L.; Browning, N. D.; Arslan, I Controlled growth of nanoparticles from solution with in situ liquid transmission electron microscopy. *Nano Lett.* **2011**, *11* (7), 2809–2813.

(25) Kelly, D. F.; Dukovski, D; Walz, T Monolayer purification: A rapid method for isolating protein complexes for single-particle electron microscopy. *Proc. Natl. Acad. Sci.U.S.A.* **2008**, *105* (12), 4703.

(26) Li, X; Zhu, Y; Cai, W; Borysiak, M; Han, B; Chen, D; Piner, R; Colombo, L; Ruoff, R. S. Transfer of Large-Area Graphene Films for High-Performance Transparent Conductive Electrodes. *Nano Lett.* **2009**, *9* (12), 4359–4363.

(27) Li, X; Magnuson, C. W.; Venugopal, A; An, J; Suk, J. W.; Han, B; Borysiak, M; Cai, W; Velamakanni, A; Zhu, Y; Fu, L; Vogel, E. M.;

Voelkl, E; Colombo, L; Ruoff, R. S. Graphene Films with Large Domain Size by a Two-Step Chemical Vapor Deposition Process. *Nano Lett.* **2010**, *10* (11), 4328–4334.

(28) Suk, J. W.; Kitt, A.; Magnuson, C. W.; Hao, Y.; Ahmed, S.; An, J; Swan, A. K.; Goldberg, B. B.; Ruoff, R. S. Transfer of CVD-Grown Monolayer Graphene onto Arbitrary Substrates. *ACS Nano* **2011**, DOI: 10.1021/nn201207c.

(29) Aleman, B; Regan, W; Aloni, S; Altoe, V; Alem, N; Girit, C; Geng, B; Maserati, L; Crommie, M; Wang, F; Zettl, A Transfer-Free Batch Fabrication of Large-Area Suspended Graphene Membranes. *ACS Nano* **2010**, *4* (8), 4762–4768.

■ NOTE ADDED AFTER ASAP PUBLICATION

This article was published ASAP on September 21, 2011. The original reference 8 has been removed. The corrected version was posted on September 28, 2011.